JACS
JOURNAL OF THE AMERICAN CHEMICAL SOCIETY

ARTICLE

pubs.acs.org/JACS

Fast Folding of RNA Pseudoknots Initiated by Laser Temperature-Jump

Ranjani Narayanan,[†,§] Yogambigai Velmurugu,[†] Serguei V. Kuznetsov,[†] and Anjum Ansari*[,†,‡]

[†]Department of Physics (M/C 273) and [‡]Department of Bioengineering (M/C 063), University of Illinois at Chicago, 845 W. Taylor St., Chicago, Illinois 60607, United States

Supporting Information

ABSTRACT: RNA pseudoknots are examples of minimal structural motifs in RNA with tertiary interactions that stabilize the structures of many ribozymes. They also play an essential role in a variety of biological functions that are modulated by their structure, stability, and dynamics. Therefore, understanding the global principles that determine the thermodynamics and folding pathways of RNA pseudoknots is an important problem in biology, both for elucidating the folding mechanisms of larger ribozymes as well as addressing issues of possible kinetic control of the biological functions of pseudoknots. We report on the folding/unfolding kinetics of a hairpin-type pseudoknot obtained with microsecond time-resolution in response to a laser temperature-jump perturbation. The kinetics are monitored using UV absorbance as well as fluorescence of extrinsically attached labels as spectroscopic probes of the transiently populated RNA conformations. We measure folding times of 1−6 ms at 37 °C, which are at least 100-fold faster than previous observations of very slow folding pseudoknots that were trapped in misfolded conformations. The measured relaxation times are remarkably similar to predictions of a computational study by Thirumalai and co-workers (Cho, S. S.; Pincus, D.L.; Thirumalai, D. *Proc. Natl. Acad. Sci. U. S. A.* **2009**, *106*, 17349−17354). Thus, these studies provide the first observation of a fast-folding pseudoknot and present a benchmark against which computational models can be refined.

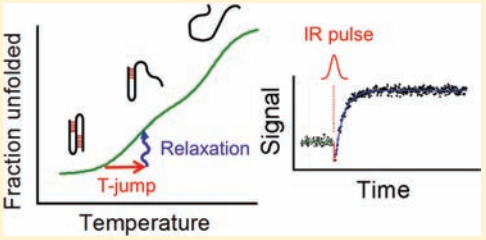

INTRODUCTION

Pseudoknots are important structural motifs in RNA molecules that bring remote parts of an RNA sequence together through base pairing between loops and other single-stranded regions to form a stable tertiary conformation. They stabilize the structures of many ribozymes and also play an essential role in a variety of biological functions that include regulating translation initiation, modulating protein elongation by stimulating ribosomal frameshifting, and maintaining human telomerase RNA activity.[1,2] Their structure, stability, and dynamics modulate their biological functions. For example, in human telomerase RNA (hTR) pseudoknot, a conformational switch between competing hairpin and pseudoknot structures plays an important functional role in the translocation of telomerase during telomere addition.[3,4] Diseases such as dyskeratosis congenital are caused by mutations in the hTR pseudoknot that affect the equilibrium among these alternative conformations.[4,5] In viral mRNA, the unfolding time scales of pseudoknot structures that cause ribosomes to pause during elongation may be one of the key factors that determine the frameshifting efficiency.[1,6,7] These and many other data point out the likely importance of kinetic control of the biological functions of many pseudoknots.

Understanding the global principles that determine the thermodynamics and folding kinetics of RNA pseudoknots is therefore an important problem in biology, both for elucidating the folding mechanisms of larger ribozymes as well as addressing issues of the role of conformational fluctuations in their biological functions. Although much has been learned about the folding thermodynamics of simple hairpin-type (H-type) pseudoknots,[1,8] including a number of important micromanipulation studies on the unfolding and refolding of pseudoknots under tension from externally applied force,[9−12] a general picture of how pseudoknots spontaneously fold is lacking. As demonstrated for nucleic acid hairpins, folding pathways and transition states may be very different in the presence and absence of applied force.[13−16] Folding/unfolding rates under external force cannot always be easily extrapolated to spontaneous events. Kinetics measurements in the absence of applied force are limited to a few studies on very slow folding pseudoknots.[17,18] Observations of some fast folding ribozymes[19−24] have highlighted a fundamental question: What are the mechanisms by which the minimal tertiary unit in RNA molecules, the pseudoknot, forms?

Folding of large RNA molecules has been described as a hierarchical process,[25] with initially a rapid collapse and formation of local secondary structure such as hairpins and bulges, followed by tertiary contacts to form subdomains, which then interact to form higher order structures with longer range tertiary contacts. What are the time scales on which each of these steps occurs? Hairpins form on time scales of tens-of-microseconds,[13,26−28] while multivalent ions mediated collapse occurs within 10 ms.[29,30] Large ribozymes with complex topologies typically fold on time

Received: June 20, 2011
Published: September 29, 2011

ACS Publications © 2011 American Chemical Society

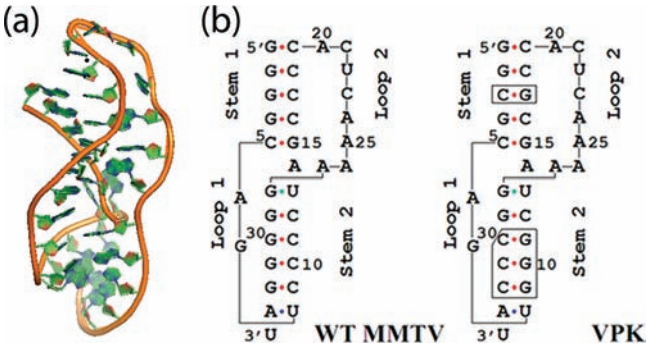

Figure 1. Secondary and tertiary structures of MMTV/VPK. (a) NMR structure of VPK pseudoknot (PDB ID: 1RNK). (b) Sequences of wild type MMTV (left) and mutant VPK (right). The regions where G:C pairs in the wild type are swapped by C:G pairs in VPK are indicated by boxes.

scales of 1−1000 s.[31,32] The bottleneck in ribozyme folding appears to be misfolded structures that act as traps in the folding energy landscape.[33−35] These traps could arise as a result of non-native base pairings at the level of secondary structure.[36,37]

That some RNA molecules can fold rapidly, within 10 ms, starting from correctly folded secondary structure, was known from the early temperature-jump (T-jump) studies on the folding of tRNA.[38,39] Recently, a number of groups have engineered modifications in the native sequence of ribozymes that help to avoid kinetic traps, leading to a number of fast-folding ribozymes.[19−22] The *Azoarcus* ribozyme is an example of a wild-type ribozyme that exhibits very rapid folding dynamics, with substantial folding within the dead-time of stopped-flow measurements.[23,24] These fast-folding molecules provide valuable insights into aspects of tertiary structure formation, such as entropic search in conformational space from prefolded secondary structure elements, that may be obscured if the rate-determining step in the folding kinetics is the unfolding from misfolded traps.

RNA pseudoknots provide an ideal playground to explore the ruggedness of the energy landscape and the interplay between competing secondary and tertiary interactions. This ruggedness is already evident in the folding of simple hairpins[13,16,40−44] and is likely more pronounced in pseudoknots, as revealed by the very slow folding kinetics observed in some isolated pseudoknots[17,18] or in the context of larger ribozymes.[45] Recent computational studies of a few H-type pseudoknots have predicted folding times of a few milliseconds,[46,47] underscoring the need to examine the folding kinetics of simple pseudoknots with minimal alternative pairings, using experimental techniques that allow submillisecond time resolution.

Here, we use nanosecond laser T-jump to rapidly perturb folded pseudoknots and monitor their relaxation kinetics. We focus on VPK (Figure 1a), a variant of the MMTV pseudoknot that promotes efficient frameshifting in mouse mammary tumor virus.[8,48,49] The VPK sequence differs from the wild-type MMTV sequence in that four of the G-C base-pairs are flipped to C-G base-pairs to disrupt G-rich tracks (Figure 1b), thus potentially avoiding alternative pairings in the stem regions. The thermodynamics of VPK pseudoknot have been extensively characterized under a range of ionic conditions.[49,50] Thermal melting is hierarchical, with first the loss of the pseudoknot structure and then the loss of the residual hairpin structure at a higher temperature, allowing us to isolate the kinetics of the transitions between the pseudoknot and the partially folded intermediate (hairpin) conformations. Our kinetics measurements provide the first observation of a fast-folding pseudoknot, with folding times of a few milliseconds, in remarkable agreement with predictions from a simulations study.[47]

EXPERIMENTAL SECTION

Samples. All RNA strands were synthesized and fluorescently labeled by Dharmacon. The extent of fluorescent labeling in F-VPK (VPK with fluorescein attached at the 5'-end) was determined by comparing the concentration of RNA strands, from UV absorbance at 260 nm (molar extinction coefficient 344 500 M^{-1} cm^{-1} for F-VPK) with direct measurements of fluorescein concentrations in the labeled strands at 494 nm, with molar extinction coefficients of 75 000 M^{-1} cm^{-1}.

Equilibrium Measurements. The steady-state absorbance and fluorescence emission spectra were measured on HP4420 spectrophotometer (Hewlett-Packard, Co., Palo Alto, CA) and FluoroMax2 or FluoroMax 3 spectrofluorimeters (Jobin Yvon, Inc., NJ), respectively. The fluorescence emission spectra were acquired with excitation of fluorescein at 495 nm.

For the absorbance measurements shown in Figure 2, two sets of measurements were averaged together, with strand concentrations of 16.8 μM for VPK and 17.2 and 45 μM for F-VPK. For the fluorescence measurements shown in Figure 3, the strand concentration was 3.8 μM for F-VPK. For the absorbance measurements on the hairpins (shown in Figure S2, Supporting Information), the strand concentrations were 30 μM for HS1 (sequence G1-C19 of VPK) and 1 μM for HS2 (sequence U8−U34 of VPK).

Analysis of Melting Profiles. All melting profiles that exhibited a single-transition were described in terms of a van't Hoff transition with linear upper and lower baselines, and two parameters describing the transition: ΔH_{vH}, the enthalpy difference between the folded and the unfolded conformations, and T_m, the melting temperature defined by the mid-point of the transition. For melting profiles that showed two transitions, the temperature dependence of the measured signal was described in terms of two sequential van't Hoff transitions as $A(T) = A_L(T) + A_1 f_1 + A_2 f_2$; here $A_L(T)$ is the lower baseline parametrized as a straight line, A_1 and A_2 are the amplitudes of the first and second transitions, respectively, and f_1 and f_2 are the fraction unfolded in each of the transitions, as described in eq 1.

$$f_i = \left(1 + \exp\left[-\frac{\Delta H_{vH,i}}{R\left(\frac{1}{T} - \frac{1}{T_{m,i}}\right)}\right]\right)^{-1} \quad (1)$$

For melting profiles exhibiting two transitions, the thermodynamic parameters were obtained from best fit to the derivative of the melting profiles, as shown in Figure 2b.

Laser Temperature-Jump Spectrometer. Rapid T-jump was achieved in sample cuvettes of path length 0.5 mm, as described previously.[51,52] The probe source for the absorbance measurements was a 200 W Hg−Xe lamp with a short-pass filter (Semrock FF01-310/SP), with >80% transmission between 260 and 290 nm, placed between the lamp and the sample, and an interference filter centered at 266 nm with 20 nm full width at half maximum (CVI H220-125), placed before the photomultiplier tube (Hamamatsu R928) that was used to measure the transmitted intensities. The probe source for the fluorescence measurements was a 20 mW cw diode laser at 488 nm (Newport PC13589), and the fluorescence emission intensities were measured with a band-pass filter (Semrock FF01-580/23), with >95% transmission between 570 and 590 nm, placed before the photomultiplier tube. Kinetic traces were typically acquired on multiple time scales, with ~20 000 data points in

each kinetic trace. The shortest time scale covered kinetics up to 200 μs, with a time-resolution of 10 ns, while the longest time scale covered kinetics up to 80 ms, with a time resolution of 4 μs. The data points prior to ~10 μs for fluorescence traces and ~100 μs for absorbance traces were discarded because of artifacts resulting from scattered laser light and/or cavitation effects. The magnitude of the T-jump was determined by fluorescence measurements on free Trp, in the setup with the Hg−Xe lamp, or fluorescein labeled unstructured single-stranded (ss) DNA, in the setup with the 488 nm diode laser, and the initial drop in the measured fluorescence emission intensity as a result of the T-jump was calibrated against steady-state measurements of the temperature-dependent change in the quantum yield of the respective fluorophore. The errors in estimating the size of the T-jump are about 10−20%.

Analysis of Kinetics Measurements. All relaxation traces are well-described by a single-exponential decay with a characteristic time constant τ_r. To account for any contribution from the recovery of the T-jump to the measured relaxation kinetics, on time scales >20 ms, we deconvoluted the T-jump recovery from the relaxation kinetics, using the following expression:[51]

$$I(t) = (I(0^+) - I(\infty))[\exp(-t/\tau_r] + (I(\infty) - I(0^-))\left[\frac{1}{1 + t/\tau_{rec}}\right] + I(0^-) \quad (2)$$

Here $I(t)$ denotes the measured signal (absorbance or fluorescence) as a function of time after the T-jump, $I(0^+)$ is the signal at $t = 0^+$ (i.e., at the beginning of the observed relaxation trace, immediately after the T-jump), $I(0^-)$ is the average signal before the T-jump, $I(\infty)$ is the signal at the end of the observed relaxation process, at $t \gg \tau_r$, and τ_{rec} is the characteristic time constant on which the T-jump recovers to the initial temperature T_i, and which was determined a priori by control measurements on free Trp or fluorescein-labeled ssDNA. The parameters that were varied in the least-squares fit to the relaxation traces were $I(0^+)$, $I(\infty)$, and the relaxation time τ_r.

To determine whether the amplitudes of the relaxation traces from T-jump measurements obtained from the exponential decay analysis, defined as $I(\infty) - I(0^+)$, are consistent with the thermodynamics, we estimated the amplitudes from the melting profiles (absorbance or fluorescence) as

$$\Delta A = A(T_f) - A(T_i)\, A_L(T_f)/A_L(T_i) \quad (3)$$

where the final temperature T_f was determined from T-jump measurements on reference samples as described above. The factor $A_L(T_f)/A_L(T_i)$ in eq 3, obtained from the temperature dependence of the lower baseline (A_L) in the melting profiles, was used to estimate any change in the fluorescence or absorbance of the sample expected in the T-jump measurements prior to the observed relaxation. For example, in the case of fluorescence measurements, the temperature-dependent change in the quantum yield of fluorescein contributes to the monotonic decrease in baseline intensity in equilibrium measurements (Figure S3, Supporting Information), and should appear as a sharp drop in the fluorescence intensity immediately after the T-jump. In absorbance measurements, the temperature-dependent change in the extent of stacking in single-stranded regions contributes to the monotonic increase in baseline absorbance in equilibrium measurements (Figure 2) and may contribute to unresolved fast components in the T-jump measurements.

An absolute comparison of the amplitudes obtained in T-jump measurements with those predicted from melting profiles requires some care to minimize errors that may be introduced from any mismatch between signals measured under equilibrium conditions in the T-jump spectrometer and those measured in the equilibrium spectrometers. In the case of fluorescence measurements, this comparison is ideally done for absolute quantum yield changes, as described by Kubelka et al.,[53] which requires measurements of a reference sample in both the T-jump and the equilibrium spectrofluorimeter. In this study, we simply multiplied the amplitudes estimated from the fluorescence melting profile for each pair of initial (T_i) and final (T_f) temperatures by a factor necessary to match the intensity $A(T_i)$ at the initial temperature, measured in the spectrofluorimeter, with the intensity $I(0^-)$ measured in the T-jump spectrometer for the corresponding kinetics trace. In the case of absorbance measurements, the amplitudes estimated from the equilibrium melting measurements were corrected for any difference in the measured concentrations in the sample used for the equilibrium measurements versus the sample used in the T-jump measurements. However, no additional corrections were made for any systematic errors that may be introduced when comparing absolute absorbance of a given sample, measured in the equilibrium spectrophotometer, versus the absorbance measured in the T-jump spectrometer, as a consequence of the combination of broad-band and interference filters used in conjunction with the Hg−Xe lamp in the T-jump apparatus.

RESULTS

Thermal Melting of VPK Pseudoknot Measured by UV Absorbance. The melting of VPK pseudoknot, measured by UV absorbance, in buffer conditions (10 mM MOPS, pH 7.0, 50 mM KCl) identical to that of a previous study,[50] is shown in Figure 2. Two transitions are observed, consistent with earlier studies,[49,50] with the tertiary structure melting at ~54 °C and then the residual hairpin melting in a second transition at ~86 °C. The absorbance melting profiles are described in terms of two sequential van't Hoff transitions, as described in the Experimental Section, and the thermodynamic parameters for each transition are summarized in Table 1.

Secondary structure prediction using Mfold[54] suggests primarily two distinct structures that are approximately isoenergetic, one with stem 1 at the 5′-end still intact (Figure S1a, Supporting Information) and another with stem 2 at the 3′-end still intact (Figure S1b, Supporting Information). A combination of these and other related structures (see Figure S1c, Supporting Information) may be present in the ensemble of residual structures that remain when the molecule loses its tertiary interactions. For comparison, we made measurements on two hairpin structures, denoted HS1 (sequence G1-C19, with stem 1 intact) and HS2 (sequence U8−U34, with stem 2 intact). The melting

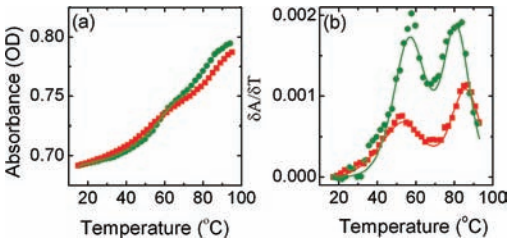

Figure 2. Melting profiles of VPK from UV absorbance measurements. (a) The absorbance of unlabeled VPK (red squares) and fluorescein-labeled F-VPK (green circles), measured at 266 nm, is plotted as a function of temperature. All measurements were carried out in 10 mM MOPS buffer, pH 7.0, 50 mM KCl. The two curves have been matched at 20 °C. (b) The first derivative of the absorbance with respect to temperature ($\delta A/\delta T$) is plotted as a function of temperature for VPK (red squares) and F-VPK (green circles). Prior to calculating the derivative, the absorbance data was smoothed over a 5 °C window. Every other data point is plotted for clarity. The continuous lines in panels (a) and (b) are fits to sequential two-step (three-state) melting.

Table 1. Thermodynamics and Kinetics Parameters for VPK and Hairpins

sample	T_m (°C)	ΔH_{vH} (kcal/mol)	τ_F[g]	τ_U[g]	$\Delta H_F^{\ddagger}$ (kcal/mol)	$\Delta H_U^{\ddagger}$ (kcal/mol)
VPK[a,b]	53.7 (86.3)	−26.7 (−52.4)	1.2 ms	11.2 ms	2.0	28.7
F-VPK[a,b]	57.2 (81.3)	−38.5 (−55.2)	–	–	–	–
F-VPK [a,c]	54.2	−25.4	5.9 ms	50.6 ms	−3.4	22.2
HS1 [a,d]	78.7	−52.4	–	–	–	–
HS2 [a,d]	70.9	−31.8	–	–	–	–
HL8-ssDNA [e]	50.5	−43.6	45.5 μs	0.87 ms	−6.1	50.1
HL9-RNA [f]	55.0	−42.6	82.0 μs	3.7 ms	9.2	52.2

[a] Buffer: 10 mM MOPS buffer, pH 7.0, 50 mM KCl. [b] Thermodynamic parameters are from UV absorbance measurements shown in Figure 2; the parameters are for the two transitions, with the second transition indicated in parentheses. [c] Thermodynamic parameters are from fluorescence measurements shown in Figure 3 and Figure S3 (Supporting Information). [d] Thermodynamic parameters are from UV absorbance measurements shown in Figure S2 (Supporting Information). [e] Buffer: 10 mM sodium phosphate, pH 7.5, 100 mM NaCl, 0.1 mM EDTA; data from ref 59. [f] Buffer: 10 mM Tris-HCl, pH 7.5, 2.5 mM $MgCl_2$; data from ref 52. [g] Folding/unfolding times at 37 °C.

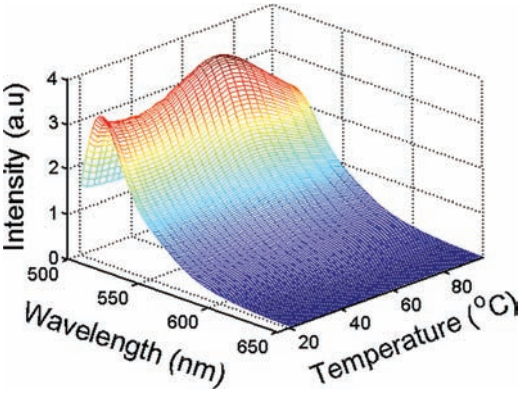

Figure 3. Melting profile of VPK from fluorescence measurements. The fluorescence emission spectra of F-VPK, with excitation at 495 nm, are plotted as a function of temperature.

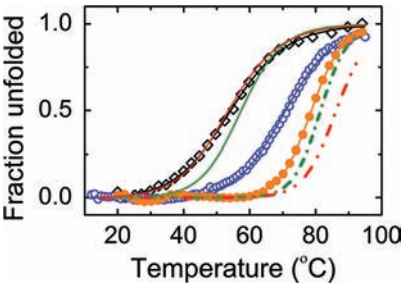

Figure 4. VPK pseudoknot and hairpin melting transitions. The fraction of unfolded pseudoknots, obtained from the fluorescence measurements on F-VPK shown in Figure 3, is plotted as a function of temperature (black open diamonds), together with the fraction of unfolded hairpins, HS1 (orange circles) and HS2 (blue open circles), obtained from the optical melting profiles shown in Figure S2 (Supporting Information). The normalized fractions for the pseudoknot/hairpin melting transitions, obtained from the UV absorbance measurements shown in Figure 2, are plotted for unlabeled VPK (red) and F-VPK (green), with the first (pseudoknot) melting transition shown with continuous lines and the second (hairpin) melting transition shown with dashed−dotted lines. All thermodynamic parameters are summarized in Table 1.

temperatures for these hairpins are ∼79 °C and ∼71 °C, respectively (Figure S2, Supporting Information).

Thermal Melting of VPK Pseudoknot Measured by Fluorescence. As an independent probe of VPK pseudoknot unfolding, we measured the fluorescence of extrinsically labeled VPK (F-VPK), with fluorescein attached at the 5′-end. The effect of the label on the pseudoknot structure is small, although not negligible, as indicated by a comparison of the transitions in VPK and F-VPK from UV absorbance measurements (Figure 2). For F-VPK, the tertiary melting transition is shifted to slightly higher temperature of ∼57 °C in comparison with unlabeled VPK, and the second transition is shifted to slightly lower temperature of ∼82 °C.

The fluorescence emission spectra of F-VPK at different temperatures, with excitation at 495 nm where fluorescein absorbs, are shown in Figure 3. F-VPK exhibits a melting transition, measured by an increase in fluorescence (Figure S3, Supporting Information), in the same temperature range as the tertiary unfolding transition measured by UV absorbance. The observed increase in fluorescence of F-VPK when the pseudoknot melts is attributed to the loss of interactions between fluorescein and the pseudoknot conformation. The fluorescence measurements are insensitive to the hairpin unfolding transition above ∼65 °C, showing only a steady drop in fluorescence owing to the drop in fluorescence quantum yield with increased temperatures. The melting profile obtained from the fluorescence emission maximum of F-VPK was analyzed in terms of a two-state van't Hoff transition (Figure S3, Supporting Information). The melting temperature thus obtained, ∼54 °C, is in very good agreement with the UV absorbance melting temperatures of ∼54 and ∼57 °C for VPK and F-VPK, respectively (see Table 1).

The fraction of unfolded pseudoknots as a function of temperature, obtained from the fluorescence measurements, is shown in Figure 4, together with the unfolded pseudoknot/hairpin fractions obtained from the UV absorbance melting profiles on VPK, F-VPK, and the two hairpins HS1 and HS2. The residual hairpin in VPK is the most stable structural element, with a melting temperature that is ∼7 °C higher than the 5′-stem hairpin HS1. The increased stability of the residual hairpin in the unfolded VPK can be attributed to the stabilizing effects of the "dangling ends" (Figure S1, Supporting Information), which are absent in the "blunt ended" hairpin stems of HS1 and HS2.[55,56]

Pseudoknot Folding/Unfolding Kinetics. To probe the kinetics of pseudoknot folding/unfolding, we measured the change in absorbance at 266 nm on unlabeled VPK and the change in fluorescence of F-VPK, in response to a laser T-jump perturbation. A typical set of kinetics traces is shown in Figure 5. For both sets of measurements, the relaxation kinetics traces are well described

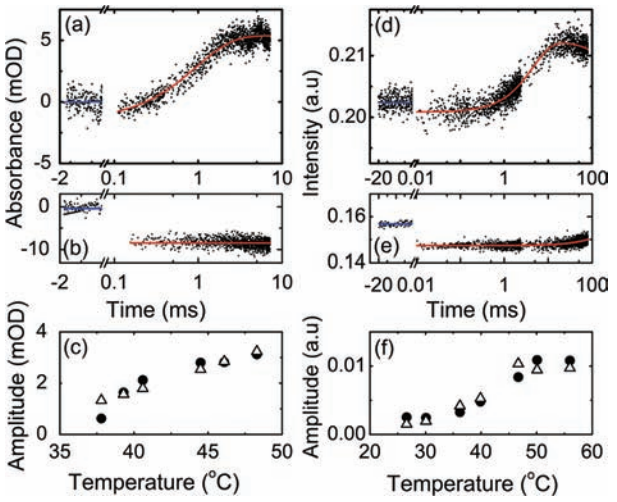

Figure 5. Relaxation kinetics of VPK. (a) The change in absorbance of unlabeled VPK (48 μM), in response to a ~4 °C T-jump from 43 to 47 °C, is plotted as a function of time. The signal prior to the laser T-jump is averaged to obtain the horizontal blue line, and all absorbance changes are calculated relative to that. The continuous red line is a single-exponential fit to the data, with relaxation time ~0.95 ms. (b) The change in absorbance of free tryptophan, in response to a ~4 °C T-jump, shows a jump in the transmitted intensity as a result of "lensing" effect from the heated volume, but no relaxation is observed on the time-scales on which VPK shows relaxation kinetics. (c) The amplitude of the relaxation kinetics, obtained from a single-exponential fit to the absorbance traces (filled circles), are plotted as a function of temperature, together with amplitudes estimated from the absorbance melting profiles, which were multiplied by a factor of 1.17 (open triangles). (d) The donor fluorescence of F-VPK (20 μM), in response to a ~6 °C T-jump from 44 to 50 °C is plotted as a function of time. The initial drop in intensity is from a change in quantum yield of the fluorescein label as a result of the T-jump. The subsequent relaxation kinetics is well-described by a single-exponential decay, with relaxation time ~4.3 ms, convoluted with the recovery of the T-jump. (e) The fluorescence of fluorescein-labeled ssDNA in response to ~6 °C T-jump from 44 to 50 °C shows the initial drop in fluorescence, followed by recovery of the T-jump, with a characteristic time constant of ~280 ms. (f) The amplitude of the relaxation kinetics, obtained from a single-exponential fit to the fluorescence traces (filled circles), is plotted as a function of temperature, together with amplitudes estimated from the fluorescence melting profiles, which were multiplied by a factor of 0.31 (open triangles).

as single-exponential decays, with time constants in the range of a few milliseconds. The corresponding control experiments (absorbance of free Trp in Figure 5b and fluorescence of fluorescein-labeled 35-nucleotide (nt) long ssDNA, previously characterized to be unstructured,[57] in Figure 5e) do not show any relaxation kinetics on these time scales; instead they show recovery of the temperature to pre-T-jump values, with a time constant of ~280 ms. Any contribution to the measured signals from the recovery of the T-jump is deconvoluted from the relaxation kinetics, as described in the Experimental Section.

To determine whether the observed relaxation kinetics capture the entire pseudoknot-to-hairpin transition expected from the thermodynamics measurements, we compared the amplitudes of the relaxation kinetics traces at different conditions of initial and final temperatures, obtained from the single-exponential fit to the decay curves, with the amplitudes estimated from the equilibrium melting profiles, for both absorbance and fluorescence measurements (Figure 5c,f), as described in the Experimental Section. For absorbance measurements, the amplitudes obtained from the relaxation traces are found to be ~17% larger than the amplitudes estimated from equilibrium measurements, over the entire temperature range for which we observed relaxation kinetics (Figure 5c). This discrepancy cannot be from "missing" amplitudes in kinetics measurements. Instead, we attribute it to errors introduced from imperfect matching of the absorbance of the sample measured in the T-jump apparatus with that measured in the equilibrium spectrophotometer, compounded with errors in accurate estimates of the final temperature after the T-jump.

For fluorescence measurements, the amplitudes obtained from the relaxation traces are significantly smaller than the amplitudes estimated from equilibrium measurements, by more than a factor of 3 (amplitudes obtained from the melting profiles are multiplied by 0.31 in Figure 5f). We attribute this discrepancy primarily to the existence of a missing, fast component with significant amplitude in the fluorescence measurements, arising from a rapid increase in fluorescence intensity within the "dead-time" of our kinetics measurements, as is evident from the observed kinetics traces at different temperatures, shown in Figure S4 (Supporting Information). The absolute amplitude of this missing phase diminishes as the initial temperature is raised, as does the fraction of pseudoknot population at equilibrium. However, the relative amplitude of this phase in comparison with the amplitude of the observed relaxation remains unchanged, as indicated by the nearly perfect agreement between the amplitudes measured from the relaxation kinetics and the scaled amplitudes estimated from the melting profile, over the entire temperature range where kinetics was measured (Figure 5f). Therefore, a plausible explanation for the missing fast phase is partial loss of interactions between the fluorescein label and the pseudoknot in a rapid "premelting" step, e.g., "fraying" at the ends, in response to the T-jump, which, if it is occurring on time scales faster than ~10 μs, would be unresolved in our kinetics measurements. The fact that the shape of the amplitudes versus temperature profile obtained from fluorescence kinetics measurements is in excellent agreement with the shape predicted from thermodynamics, together with our observation that the absorbance measurements show no evidence for any missing phases, indicates that we are indeed measuring the folding/unfolding kinetics corresponding to the pseudoknot-to-hairpin transition that is observed in the thermodynamics measurements.

The temperature dependence of the relaxation times obtained for VPK and F-VPK is shown in Figure 6. The two sets of measurements yield similar, though not identical, relaxation times for the tertiary folding/unfolding; the relaxation times for VPK are ~5-fold faster than for F-VPK. This difference may be attributed in part to the effect of the fluorescent label on the stability and folding pathway of the pseudoknot. The folding/unfolding times can be extracted from the measured relaxation times and the van't Hoff equilibrium parameters, assuming a two-state transition. The folding (τ_F) and unfolding (τ_U) times at 37 °C, together with the corresponding activation enthalpies ($\Delta H_F^{\ddagger}$ and $\Delta H_U^{\ddagger}$), obtained from an Arrhenius fit to the folding/unfolding times, are summarized in Table 1.

DISCUSSION

The present study was conducted to investigate how rapidly RNA pseudoknot structures are formed under conditions where

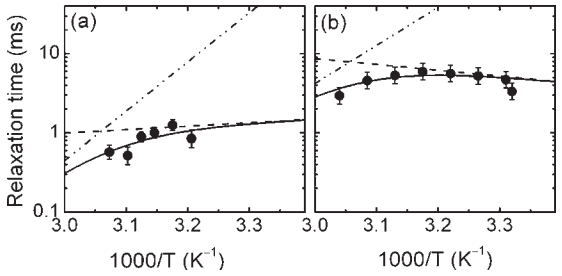

Figure 6. Temperature dependence of relaxation times. The relaxation times obtained from single-exponential fits to the kinetics traces in (a) absorbance measurements on VPK and (b) fluorescence measurements on F-VPK are plotted as a function of inverse temperature. The error bars represent standard deviations from the average of three measurements for the absorbance data and two measurements for the fluorescence data. The continuous black lines are the best fit to the relaxation times obtained from a two-state analysis, with the folding and unfolding times shown as dashed and dashed−dotted lines, respectively, described in terms of an Arrhenius dependence, with fit parameters summarized in Table 1.

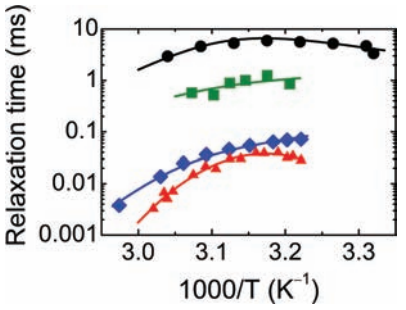

Figure 7. Relaxation times of pseudoknots and hairpins. The relaxation times obtained from absorbance measurements on VPK (green squares) and fluorescence measurements on F-VPK (black circles) are plotted versus inverse temperature. For comparison, the relaxation times obtained for a 5-bp stem, 9-nt loop RNA hairpin (HL9-RNA, blue diamonds) and a 7-bp stem, 8-nt loop ssDNA hairpin (HL8-ssDNA, red triangles) are also plotted. The continuous lines are the best fit from a two-state analysis.

misfolding in non-native structures is minimized. Two factors contribute to the avoidance of stable misfolded structures in this study. The first is the RNA sequence of VPK, which was designed to avoid significant stretches of mispaired stems.[48] The second is the design of the experiment itself, in which a T-jump perturbs the tertiary interactions but does not necessarily completely unfold the RNA secondary structure. This is evident from the hierarchical melting observed for VPK.[49,50] Under monovalent ionic conditions of the present study (~50 mM K^+), two distinct unfolding transitions, corresponding to first the loss of tertiary interactions and then the loss of the residual secondary structure, are observed, consistent with previous UV absorbance as well as differential scanning calorimetry (DSC) measurements.[49,50] All kinetics measurements reported here were obtained at temperatures below ~60 °C, where negligible signal is expected from the melting of the residual hairpin structures.

The folding times of ~1−6 ms at 37 °C reported here for VPK are significantly smaller than previous measurements of pseudoknot folding times, which ranged from 350 ms to minutes.[17,45,58] The very slow folding observed in these earlier studies was attributed to mispaired stems that can be quite stable at temperatures below their T_m. Recently, a few studies have reported folding/unfolding kinetics of H-type pseudoknots under mechanical tension.[9−12] The measured rates are well-described in terms of an exponential dependence on force, of the form $k(F) = k_0 \exp(F\Delta x^{\ddagger}/k_BT)$, where $\Delta x^{\ddagger}$ is the distance to the transition state. However, k_0 does not always correspond to the actual rates under conditions of zero force, because the position of the transition state itself may be force dependent.[11] As an illustration, mechanical unfolding measurements on a frame-shifting pseudoknot from infectious bronchitis virus (IBV), carried out over a force range of 15−20 pN, yield apparent folding and unfolding times at zero force of ~1.8 μs and ~8000 s, respectively.[11]

In another mechanical unfolding study,[9] on hTR pseudoknot, which revealed a stepwise formation of the pseudoknot at low forces with one stem forming before the other, measurements at forces below 6 pN allowed the hairpin-to-pseudoknot (H−P) transition to be studied separately from the completely unfolded (single-stranded) to hairpin (S−P) transition, in a manner similar in nature to the T-jump measurements reported here. These measurements yield folding times for H−P transition in hTR of ~8.3 s at 5 pN, with an extrapolated value of ~60 ms at zero force, which is 10−60-fold slower than the folding of VPK observed in this study. It remains to be determined whether folding of hTR is indeed slower than that of VPK, when measured under identical conditions.

It is informative to compare VPK folding/unfolding times with corresponding measurements on nucleic acid hairpins. Figure 7 shows the relaxation times obtained with T-jump measurements on VPK (this study) and on two hairpins, a 7-bp stem, 8-nt loop single-stranded DNA hairpin,[59] denoted here as HL8-ssDNA, and a 5-bp stem, 9-nt loop RNA hairpin,[52] denoted here as HL9-RNA. A striking result is the 10−100-fold slower folding of VPK pseudoknot in comparison with hairpins. There are also some notable similarities. First, hairpins and pseudoknots exhibit qualitatively similar dependence of relaxation times on temperature, with negative or negligible activation enthalpies for the folding step and large, positive activation enthalpies for the unfolding step. All ssDNA and RNA hairpins that we have examined under T-jump conditions in earlier studies with the exception of HL9-RNA show negative activation enthalpies for the folding step.[13,52,60] Negative activation enthalpies are also observed in the folding of β-hairpins in polypeptides.[61] Second, the activation enthalpies for the unfolding step are comparable in magnitude to the equilibrium enthalpy change (Table 1). All together, these results point to an entropic barrier as the dominant contributor to the bottleneck for folding of both hairpins and pseudoknots. In the case of hairpins, this free energy barrier is primarily the entropic cost of loop formation.[13,62,63]

The question arises whether we can explain the significantly slower folding of pseudoknots by a corresponding increase in the free energy of loops in pseudoknots (ΔG^{P}_{loop}), in comparison with loops in hairpins (ΔG^{H}_{loop}). For hairpins, we estimate the entropy of loops from the Shimada−Yamakawa expression for loop-closure probability for a wormlike chain.[64] For a 9-nt loop of length 6 nm and persistence length 1 nm, we obtain $\Delta G^{H}_{loop} \approx$ 2.3 kcal/mol.[52,62] Our experimental folding times for VPK pseudoknot are a factor of 15−70 slower than that of HL9-RNA hairpin (Figure 7 and Table 1). If the slower folding of pseudoknots is attributed primarily to an increased entropic

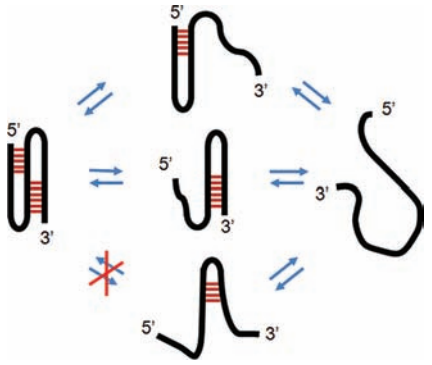

Figure 8. Folding/unfolding pathways of H-type pseudoknots. A schematic of different folding pathways for pseudoknots is illustrated, with partially folded structures such as the 5′-stem hairpin, the 3′-stem hairpin, or a misfolded hairpin.

barrier, we estimate $\Delta G^{P}_{loop} \approx 4.0 - 4.9$ kcal/mol. On the basis of our observation that F-VPK folding is 5-fold slower than that of VPK, it is tempting to suggest that the unfolding/refolding pathways are not identical for the labeled and unlabeled VPK and that the presence of the label in F-VPK perturbs the thermodynamics in such as way as to tilt the balance in favor of a different stem to unfold first in comparison with the unlabeled VPK. Parallel folding pathways have been observed in coarse-grained computational studies of RNA pseudoknot folding kinetics,[47] as illustrated in Figure 8, which includes possible "off-pathway" traps. Evidence for traps in the folding pathway of H-type pseudoknots, with "non-native" Watson–Crick pairs that needed to be disrupted for the pseudoknot to fold, came from an earlier experimental study by Tinoco and co-workers.[17] Further experimental studies are needed to examine in detail the folding/refolding pathways of VPK.

Theoretical estimates for loop entropies of pseudoknots remain a challenge and an area of intense research.[65−69] The difficulty lies in correctly accounting for the conformational space accessible to loops in pseudoknots, because of stem-loop correlations that make the loop entropy calculation very complex. Empirical estimates of ΔG^{P}_{loop} have been proposed by Gultyaev et al.,[65] who have provided a useful table of numerical values at 37 °C, for loops and stems of various lengths. They obtain $\Delta G^{P}_{loop} \approx 4.2$ kcal/mol for a 6-bp long 3′-stem (stem 2) interacting with 2-nt loop 1 and $\Delta G^{P}_{loop} \approx 6.4$ kcal/mol for a 5-bp long 5′-stem (stem 1) interacting with 8-nt loop 2. Another estimate comes from Cao and Chen,[68] who obtain $\Delta G^{P}_{loop} \approx 2.7$ kcal/mol for a 6-bp long 3′-stem (stem 2) interacting with 2-nt loop 1 and $\Delta G^{P}_{loop} \approx 5.5$ kcal/mol for a 5-bp long 5′-stem (stem 1) interacting with 8-nt loop 2. Our experimental estimates of ΔG^{P}_{loop}, based on kinetics measurements, hold promise for further fine-tuning of both theory and experimental interpretation.

How do our experimental results compare with theoretical predictions of the folding kinetics of H-type pseudoknots? Simulations carried out by Thirumalai and co-workers, using coarse-grained models of RNA, have successfully captured the salient features of the thermodynamics of VPK and other simple H-type pseudoknots.[47] More importantly, these simulations make detailed predictions regarding the folding time scales and pathways. For VPK, these studies predict parallel folding pathways with 77% molecules folding via stem1→stem2 pathway and 23% molecules folding via stem2→stem1 pathway, with time constants of 0.4 and 4.3 ms, respectively. In another simulations study, by Cao and Chen,[46] on the hTR pseudoknot, a significant reduction in folding times is predicted for the ΔU177 mutant in comparison with the wild-type hTR. Their detailed predictions of folding time scales and pathways have yet to be verified by direct experiments. Our measurements are a first step in this direction, with our results on VPK folding times in remarkably good agreement with some of the predictions of the Thirumalai group.[47]

CONCLUSIONS

The folding/unfolding kinetics measurements on VPK pseudoknot presented here represents the first observation of a fast-folding pseudoknot under spontaneous folding conditions, with folding times of a few milliseconds. These time scales are at least 100-fold faster than previous observations of pseudoknot folding and raise an important question as to whether the rapid kinetics observed in T-jump measurements are the result of refolding from correctly preformed "on-pathway" secondary structures. Whether the folding will follow kinetic partitioning if initiated from a completely unfolded structure, with a fraction of rapidly folding population that avoids traps and the remaining fraction that gets stuck in misfolded conformations and folds slowly,[70] remains to be determined. In any event, the possibility of isolating the fast-folding population using T-jump techniques holds promise for gaining new insights into the conformational search problem intrinsic to the folding of RNA pseudoknots from prefolded secondary structure elements and for providing experimental estimates of the entropic barriers to the folding process, thus aiding computational models for structure prediction and folding mechanisms. These measurements open up avenues that, in synergy with computational studies, will help unravel the folding pathways and the underlying energetics of RNA pseudoknots in some detail.

ASSOCIATED CONTENT

Supporting Information. Figure S1, low-energy secondary structures of VPK predicted by Mfold; Figure S2, absorbance melting profiles of hairpins HS1 and HS2; Figure S3, fluorescence melting profile of F-VPK; Figure S4, representative kinetics traces obtained from fluorescence measurements on F-VPK. This material is available free of charge via the Internet at http://pubs.acs.org.

AUTHOR INFORMATION

Corresponding Author
ansari@uic.edu

Present Addresses
[§]School of Physical and Mathematical Sciences, Division of Chemistry & Biological Chemistry, Nanyang Technological University, Singapore.

ACKNOWLEDGMENT

This research was supported by the National Science Foundation (MCB-0721937). We thank Dave Thirumalai for helpful discussions.

REFERENCES

(1) Giedroc, D. P.; Theimer, C. A.; Nixon, P. L. *J. Mol. Biol.* **2000**, *298*, 167.

(2) Dam, E.; Pleij, K.; Draper, D. *Biochemistry* **1992**, *31*, 11665.
(3) Comolli, L. R.; Smirnov, I.; Xu, L.; Blackburn, E. H.; James, T. L. *Proc. Natl. Acad. Sci. U. S. A.* **2002**, *99*, 16998.
(4) Theimer, C. A.; Finger, L. D.; Trantirek, L.; Feigon, J. *Proc. Natl. Acad. Sci. U. S. A.* **2003**, *100*, 449.
(5) Chen, J. L.; Greider, C. W. *Trends Biochem. Sci.* **2004**, *29*, 183.
(6) Brierley, I.; Pennell, S.; Gilbert, R. J. *Nat. Rev. Microbiol.* **2007**, *5*, 598.
(7) Giedroc, D. P.; Cornish, P. V. *Virus Res.* **2009**, *139*, 193.
(8) Chen, X.; Chamorro, M.; Lee, S. I.; Shen, L. X.; Hines, J. V.; Tinoco, I., Jr.; Varmus, H. E. *EMBO J.* **1995**, *14*, 842.
(9) Chen, G.; Wen, J. D.; Tinoco, I., Jr. *RNA* **2007**, *13*, 2175.
(10) Hansen, T. M.; Reihani, S. N.; Oddershede, L. B.; Sorensen, M. A. *Proc. Natl. Acad. Sci. U. S. A.* **2007**, *104*, 5830.
(11) Green, L.; Kim, C. H.; Bustamante, C.; Tinoco, I., Jr. *J. Mol. Biol.* **2008**, *375*, 511.
(12) Chen, G.; Chang, K. Y.; Chou, M. Y.; Bustamante, C.; Tinoco, I., Jr. *Proc. Natl. Acad. Sci. U. S. A.* **2009**, *106*, 12706.
(13) Ansari, A.; Kuznetsov, S. V.; Shen, Y. *Proc. Natl. Acad. Sci. U. S. A.* **2001**, *98*, 7771.
(14) Liphardt, J.; Onoa, B.; Smith, S. B.; Tinoco, I., Jr.; Bustamante, C. *Science* **2001**, *292*, 733.
(15) Cocco, S.; Marko, J. F.; Monasson, R. *Eur. Phys. J. E.* **2003**, *10*, 153.
(16) Hyeon, C.; Thirumalai, D. *J. Am. Chem. Soc.* **2008**, *130*, 1538.
(17) Wyatt, J. R.; Puglisi, J. D.; Tinoco, I., Jr. *J. Mol. Biol.* **1990**, *214*, 455.
(18) Gluick, T. C.; Gerstner, R. B.; Draper, D. E. *J. Mol. Biol.* **1997**, *270*, 451.
(19) Rook, M. S.; Treiber, D. K.; Williamson, J. R. *J. Mol. Biol.* **1998**, *281*, 609.
(20) Buchmueller, K. L.; Webb, A. E.; Richardson, D. A.; Weeks, K. M. *Nat. Struct. Biol.* **2000**, *7*, 362.
(21) Pan, J.; Deras, M. L.; Woodson, S. A. *J. Mol. Biol.* **2000**, *296*, 133.
(22) Fang, X. W.; Thiyagarajan, P.; Sosnick, T. R.; Pan, T. *Proc. Natl. Acad. Sci. U. S. A.* **2002**, *99*, 8518.
(23) Rangan, P.; Masquida, B.; Westhof, E.; Woodson, S. A. *Proc. Natl. Acad. Sci. U. S. A.* **2003**, *100*, 1574.
(24) Rangan, P.; Masquida, B.; Westhof, E.; Woodson, S. A. *J. Mol. Biol.* **2004**, *339*, 41.
(25) Brion, P.; Westhof, E. *Annu. Rev. Biophys. Biomol. Struct.* **1997**, *26*, 113.
(26) Gralla, J.; Crothers, D. M. *J. Mol. Biol.* **1973**, *73*, 497.
(27) Porschke, D. *Biophys. Chem.* **1974**, *1*, 381.
(28) Bonnet, G.; Krichevsky, O.; Libchaber, A. *Proc. Natl. Acad. Sci. U. S. A.* **1998**, *95*, 8602.
(29) Russell, R.; Millett, I. S.; Tate, M. W.; Kwok, L. W.; Nakatani, B.; Gruner, S. M.; Mochrie, S. G.; Pande, V.; Doniach, S.; Herschlag, D.; Pollack, L. *Proc. Natl. Acad. Sci. U. S. A.* **2002**, *99*, 4266.
(30) Woodson, S. A. *Annu. Rev. Biophys.* **2010**, *39*, 61.
(31) Sclavi, B.; Sullivan, M.; Chance, M. R.; Brenowitz, M.; Woodson, S. A. *Science* **1998**, *279*, 1940.
(32) Swisher, J. F.; Su, L. J.; Brenowitz, M.; Anderson, V. E.; Pyle, A. M. *J. Mol. Biol.* **2002**, *315*, 297.
(33) Pan, J.; Thirumalai, D.; Woodson, S. A. *J. Mol. Biol.* **1997**, *273*, 7.
(34) Pan, T.; Sosnick, T. R. *Nat. Struct. Biol.* **1997**, *4*, 931.
(35) Treiber, D. K.; Rook, M. S.; Zarrinkar, P. P.; Williamson, J. R. *Science* **1998**, *279*, 1943.
(36) Wu, M.; Tinoco, I., Jr. *Proc. Natl. Acad. Sci. U. S. A.* **1998**, *95*, 11555.
(37) Thirumalai, D. *Proc. Natl. Acad. Sci. U. S. A.* **1998**, *95*, 11506.
(38) Cole, P. E.; Crothers, D. M. *Biochemistry* **1972**, *11*, 4368.
(39) Crothers, D. M.; Cole, P. E.; Hilbers, C. W.; Shulman, R. G. *J. Mol. Biol.* **1974**, *87*, 63.
(40) Zhang, W.; Chen, S. J. *Proc. Natl. Acad. Sci. U. S. A.* **2002**, *99*, 1931.
(41) Ansari, A.; Shen, Y.; Kuznetsov, S. V. *Phys. Rev. Lett.* **2002**, *88*, 069801.
(42) Jung, J.; Van Orden, A. *J. Am. Chem. Soc.* **2006**, *128*, 1240.
(43) Ma, H.; Proctor, D. J.; Kierzek, E.; Kierzek, R.; Bevilacqua, P. C.; Gruebele, M. *J. Am. Chem. Soc.* **2006**, *128*, 1523.
(44) Ma, H.; Wan, C.; Wu, A.; Zewail, A. H. *Proc. Natl. Acad. Sci. U. S. A.* **2007**, *104*, 712.
(45) Chadalavada, D. M.; Senchak, S. E.; Bevilacqua, P. C. *J. Mol. Biol.* **2002**, *317*, 559.
(46) Cao, S.; Chen, S. J. *J. Mol. Biol.* **2007**, *367*, 909.
(47) Cho, S. S.; Pincus, D. L.; Thirumalai, D. *Proc. Natl. Acad. Sci. U. S. A.* **2009**, *106*, 17349.
(48) Shen, L. X.; Tinoco, I., Jr. *J. Mol. Biol.* **1995**, *247*, 963.
(49) Gonzalez, R. L., Jr.; Tinoco, I., Jr. *J. Mol. Biol.* **1999**, *289*, 1267.
(50) Theimer, C. A.; Giedroc, D. P. *RNA* **2000**, *6*, 409.
(51) Vivas, P.; Kuznetsov, S. V.; Ansari, A. *J. Phys. Chem. B* **2008**, *112*, 5997.
(52) Kuznetsov, S. V.; Ren, C.; Woodson, S. A.; Ansari, A. *Nucleic Acids Res.* **2008**, *36*, 1098.
(53) Kubelka, J.; Eaton, W. A.; Hofrichter, J. *J. Mol. Biol.* **2003**, *329*, 625.
(54) Zuker, M. *Nucleic Acids Res.* **2003**, *31*, 3406.
(55) Sugimoto, N.; Kierzek, R.; Turner, D. H. *Biochemistry* **1987**, *26*, 4554.
(56) Bommarito, S.; Peyret, N.; SantaLucia, J., Jr. *Nucleic Acids Res.* **2000**, *28*, 1929.
(57) Kuznetsov, S. V.; Sugimura, S.; Vivas, P.; Crothers, D. M.; Ansari, A. *Proc. Natl. Acad. Sci. U.S.A.* **2006**, *103*, 18515.
(58) Zhang, L.; Bao, P.; Leibowitz, M. J.; Zhang, Y. *RNA* **2009**, *15*, 1986.
(59) Ansari, A.; Kuznetsov, S. V. *J. Phys. Chem. B.* **2005**, *109*, 12982.
(60) Ansari, A.; Kuznetsov, S. V. In *Biological Nanostructures and Applications of Nanostructures in Biology: Electrical, Mechanical & Optical Properties*; Stroscio, M. A., Dutta, M., Eds.; Kluwer Academic Publishers: New York, 2004, p 99.
(61) Munoz, V.; Thompson, P. A.; Hofrichter, J.; Eaton, W. A. *Nature* **1997**, *390*, 196.
(62) Kuznetsov, S. V.; Shen, Y.; Benight, A. S.; Ansari, A. *Biophys. J.* **2001**, *81*, 2864.
(63) Shen, Y.; Kuznetsov, S. V.; Ansari, A. *J. Phys. Chem. B.* **2001**, *105*, 12202.
(64) Shimada, J.; Yamakawa, H. *Macromolecules* **1984**, *17*, 689.
(65) Gultyaev, A. P.; van Batenburg, F. H.; Pleij, C. W. *RNA* **1999**, *5*, 609.
(66) Rivas, E.; Eddy, S. R. *J. Mol. Biol.* **1999**, *285*, 2053.
(67) Dirks, R. M.; Pierce, N. A. *J. Comput. Chem.* **2004**, *25*, 1295.
(68) Cao, S.; Chen, S. J. *Nucleic Acids Res.* **2006**, *34*, 2634.
(69) Zhang, J.; Dundas, J.; Lin, M.; Chen, R.; Wang, W.; Liang, J. *RNA* **2009**, *15*, 2248.
(70) Thirumalai, D.; Lee, N.; Woodson, S. A.; Klimov, D. *Annu. Rev. Phys. Chem.* **2001**, *52*, 751.